JOURNAL OF MATERIALS SCIENCE 27 (1992) 485–498

Dissolution process of surface oxide film during diffusion bonding of metals

Y. TAKAHASHI*, T. NAKAMURA, K. NISHIGUCHI
Department of Welding and Production Engineering, Osaka University, 11-1 Mihogaoka Ibaraki, Osaka 565, Japan

Two models of the dissolution process of surface oxide film in metals (copper and titanium) are described in order to estimate the dissolution time t_s required for the oxide film to dissolve in the metals completely. One is based on impurity diffusion (model 1). The other is given by reaction diffusion (model 2). Model 1 was applied to estimate t_s in copper and α-titanium but model 2 for t_s of β-titanium because of the formation of α-phase. In these models, the dissolution process is assumed to be controlled by the oxygen diffusion in metals. Bonding tests were performed in order to verify the calculated results. The experimental results suggest that model 1 is valid in Cu–Cu bonding. Also, as for β-titanium, no retardation of the bonding process was observed. This was in agreement with model 2. However, for α-titanium below 1000 K, the retardation time was much longer than the dissolution time calculated by model 1, i.e. the retardation below 1000 K cannot be dictated by the diffusion-controlled process. A new model is therefore proposed. The dissociation rate of the oxide film is taken into account in the new model. This new model can explain the retardation of the bonding process.

1. Introduction

Theoretical analyses of diffusion bonding of metals [1, 2] and metal powder sintering [3] have been largely based on models assuming ideal clean surfaces, that is, surface contamination (mainly surface oxide film) has usually been neglected. However, it has been widely accepted that the surface oxide film has a large influence on diffusion bonding [4–7] and sintering [8–10]. The influence depends on the behaviour of the oxide film during bonding [11, 12] which can be indicated by thermodynamic and kinetic considerations. If process conditions can be selected so that the oxide film is made thermodynamically unstable, diffusion bonding progresses under no influence of the surface oxide film. In contrast, for the diffusion bonding of metals with high oxide stability and low oxygen solubility such as aluminium, the bonding process is quite different to that of the idealized models [10, 13], because the oxide film remains stable on the bond-interface during bonding [12]. We then see that the joint exhibits a brittle fractured surface without dimples [8, 10] and the joints are often rather poor [4, 5].

On the other hand, in the diffusion bonding of metals with high oxygen solubility such as titanium, we can get the oxide layer gradually dissolving as oxygen in the metal, even if the oxide is stable by itself with respect to dissociation or reduction [9, 14]. We then observe the retardation of bulk–bulk bonding owing to the oxide layer, i.e. the bonding process is preceded by an incubation period dictated by the kinetics of dissolution of the oxygen. The actual diffusion bonding of many metals (iron, nickel, copper, etc.) and alloys (e.g. stainless steels) involves the dissolution of the oxide film into parent metal to obtain good joints [4, 11]. The dissolution process of the oxide film is, therefore, important to achieve high reliability of the diffusion-bonded joints.

The dissolution of the oxide layer involves two steps at least, that is, the first step is the dissociation of the oxide ($MO \rightarrow M + O$, where MO is the oxide of the metal M). This reaction can easily occur if the oxide is less stable as a phase than a solid solution of oxygen in metal. The second step is oxygen diffusion to the bulk.

If the dissolution process of the oxide film is controlled by oxygen diffusion, we can estimate the dissolution time taken for the oxide film to dissolve completely. However, we have only one theoretical analysis concerning the estimation of the dissolution time during diffusion bonding. This analysis was given by Munir [6, 13]. He indicated the critical thickness of the oxide films which can dissolve as oxygen in metals. Munir's analysis was essentially based on the premise of a diffusion-controlled dissolution process and the diffusing oxygen was treated as an impurity of the metal (it is sufficient to consider only the concentration gradient of the oxygen itself in the diffusion process [15]).

However, Munir has not experimentally verified his theoretical analysis. We need to confirm it because a dissolution process controlled by oxygen diffusion is not always satisfied. If the dissociation step of the oxide film does not easily occur, we need to modify the model by coupling the dissociation and diffusion (series operation model).

Moreover, in metals such as β-titanium, we know that α-phase formation occurs during diffusion, as

* *Present address*: Welding Research Institute of Osaka University, Ibaraki, Osaka 567, Japan.

0022–2461/92 $03.00 + .12

indicated by the equilibrium diagram of the Ti–O system. Thus, we need to take account of reaction diffusion [16, 17].

In the present paper, we first describe two different models to predict the dissolution time for any particular thickness of oxide film. One is similar to Munir's model (model 1). The other is based on the theory of reaction diffusion (model 2). We verify these two models experimentally. We examine the behaviour of the oxide film (the change in morphology) during bonding for the purpose of understanding the actual dissolution process. In discussion, we will propose another model (the series operation model) on the basis of the experimental results for α-titanium.

2. Models

The dissolution process of the oxide film consists of two different steps represented by

$$M_xO_y \rightarrow xM + yO^* \quad (1)$$

at the interface between the oxide film and the metal, and

$$O^* \rightarrow O_{sol} \quad (2)$$

where M_xO_y is the oxide. M the metal, x and y the numbers to express the ratio of M and O in the oxide, O* the oxygen atom at the interface, and O_{sol} the dissolved oxygen as a solute in the metal M. Equation 1 is the dissociation process of the oxide film and Equation 2 the dissolution process of O*. The second step is essentially controlled by the diffusion of O_{sol} from the original interface into the underlying metal because O* must be activated. These processes occur in series. Thus, the slower process becomes the rate-determining step [18].

At first, we assume an oxygen-diffusion-controlled dissolution process.

2.1. Model 1

Fig. 1 schematically illustrates model 1 which is based on impurity diffusion. The origin of the axis x is always taken at the interface between the oxide film and the metal. C_{ox} is the oxygen content in the oxide film. C_s the oxygen solubility of the metal, C_o the initial oxygen content of the bulk, and δ_{ox} the initial thickness of the oxide film. It is assumed that the oxide film does not escape to the outside by vapourization (sublimation), i.e. the destruction of the oxide film is performed only by assimilation into the metal.

The initial and boundary conditions are indicated in Fig. 1, i.e. at time $t = 0$ the concentration of oxygen $C = C_o$ at $x > 0$ and $C = C_s$ at $x = 0$, and also when $t > 0$, $C = C_s$ at $x = 0$ and $C = C_o$ at $x = \infty$. From Fick's law [19] we obtain the solution represented by

$$C(x, t) = (C_s - C_o)\left[1 - \mathrm{erf}\left(\frac{x}{2(Dt)^{1/2}}\right)\right] \quad (3)$$

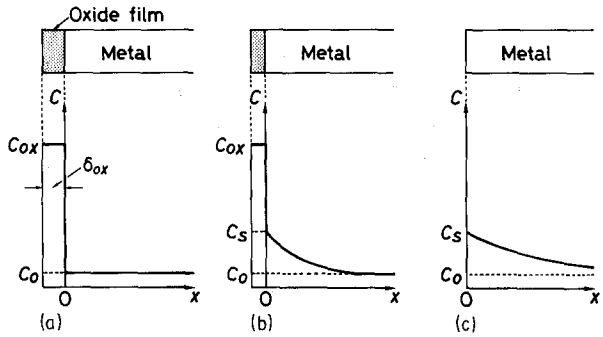

Figure 1 Schematic illustration of model 1: (a) initial condition ($t = 0$), (b) during the dissolution of oxide film ($0 < t < t_s$), (c) when the oxide film disappears ($t = t_s$).

where D is the diffusion coefficient of the oxygen in metal, erf(z) the error function, and $C(x, t)$ is the molar concentration (molarity) of the oxygen. D is expressed by $D_o\exp(-Q/RT)$ where D_o is the frequency factor, Q the activation energy, R the gas constant and T the absolute temperature. The molarity C is equal to $(C_w/100)(\rho/M_o)$ where C_w is the weight percentile concentration of oxygen, ρ the density of the material and M_o the atomic weight of oxygen. Assume that both D and ρ are constant against the concentration*. The atom flux is expressed by

$$J(x, t) = (C_s - C_o)\left(\frac{D}{\pi t}\right)^{1/2} \exp\left(-\frac{x^2}{4Dt}\right) \quad (4)$$

After integration of $J(0, t)$ with respect to t we obtain for the total quantity of diffusing oxygen having crossed unit area of the interface

$$M_t = 2\left(\frac{Dt_s}{\pi}\right)^{1/2}(C_s - C_o) \quad (5)$$

where t_s the time required for the oxide film to dissolve in metal completely. The molar quantity of oxygen within the oxide film (per unit area) is expressed by

$$m = \frac{\rho_{ox}\delta_{ox}}{M_{ox}}y \quad (6)$$

where ρ_{ox} is the density of the oxide film, M_{ox} the molar weight of the oxide and y the number in the chemical formula M_xO_y†.

From $M_t = m$, we can obtain the dissolution time by model 1 expressed by

$$t_s = \frac{\pi}{D}\left(\frac{m}{2(C_s - C_o)}\right)^2 \quad (7)$$

2.2. Model 2

Fig. 2 schematically illustrates reaction diffusion between the oxide film and the β-phase, where the α-phase is newly formed.

The rate equations for reaction diffusion in the binary system have been given elsewhere [16, 17,

* For a metal with low oxygen solubility such as copper, we can regard D and ρ as constant against the concentration. For titanium, they may be variable with the concentration because titanium has a high oxygen solubility. However, in the present study we assume that D and ρ are constant for titanium.

† We regarded copper and titanium oxide films as CuO and TiO, respectively, i.e. $y = 1$. For Cu_2O, δ_{ox} is 1.915 times as large as that of CuO for the same molar amount of oxygen. δ_{ox} of TiO_2 is 0.725 times as large as that of TiO.

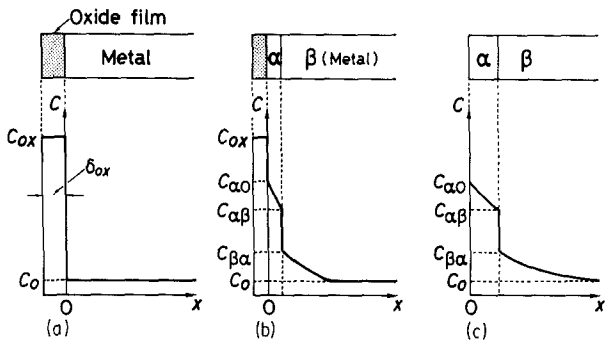

Figure 2 Schematic illustration of model 2: (a) initial condition ($t=0$), (b) formation of α-phase by dissolution of oxide film ($0<t<t_s$), (c) when the oxide film disappears ($t=t_s$).

20, 21]. According to them, the width of the ith phase is in proportion to the square root of time, i.e.

$$\Delta x_i = k_i t^{1/2} \tag{8}$$

where k_i is constant for layer growth of the ith phase. Here, we can assume that the concentration gradient in each phase is always constant, because Δx_i is small enough. We then obtain the equation

$$16D_i(\tilde{C}_{i,i-1} - \tilde{C}_{i,i+1}) = k_i \sum_{j=1}^{n} \alpha_{ij} k_j \tag{9}$$

where D_i is the interdiffusion coefficient at the ith phase (exactly speaking, the interdiffusion coefficient at $\tilde{C} = \tilde{C}_i^*$ as indicated in Fig. 3a), $\tilde{C}$ is the normalized concentration defined as $(C - C_o)/(C_{ox} - C_o)$, $\tilde{C}_{ij}$ the normalized concentration of the ith phase adjacent to the jth phase (see Fig. 3a) and n the total number of phases; α_{ij} is given by

$$\alpha_{ij} = 2(\tilde{C}_{i,i-1} + \tilde{C}_{i,i+1}) \times (2 - \tilde{C}_{j,j-1} - \tilde{C}_{j,j+1}) \tag{10}$$

for $1 \leqslant j < i$,

$$\alpha_{ij} = 5\tilde{C}_{i,i+1} + 3\tilde{C}_{i,i-1} - 2(\tilde{C}_{i,i-1} + \tilde{C}_{i,i+1})^2 \tag{11}$$

for $i = j$, and

$$\alpha_{ij} = 2(2 - \tilde{C}_{i,i-1} - \tilde{C}_{i,i+1}) \times (\tilde{C}_{j,j-1} + \tilde{C}_{j,j+1}) \tag{12}$$

for $i < j \leqslant n$.

In the system of TiO–β-Ti, the phase of α-titanium just grows (see Fig. 4b). We need to consider the case of $n = 3$ which is shown in Fig. 3b. If the initial width of the oxide is large enough, Equation 9 is always valid. However, the oxide film is usually thin. We must assume that the oxygen content in the oxide film is always constant, that is $\tilde{C}_{ox} = \tilde{C}_{01} = \tilde{C}_{12} = 1$, or $k_1 = 0$ ($D_1 \ll D_2$ and $D_1 \ll D_3$ in Fig. 3b). This means that the diffusion layer within the oxide film does not appear ($\Delta x_1 = 0$). Namely, it follows that the thickness of the oxide film monotonously decreases with time.

For $n = 3$, Equation 9 is therefore rewritten as

$$16D_1(\tilde{C}_{10} - \tilde{C}_{12}) = k_1(\alpha_{11}k_1 + \alpha_{12}k_2 + \alpha_{13}k_3) = 0 \tag{13}$$

$$16D_2(\tilde{C}_{21} - \tilde{C}_{23}) = k_2(\alpha_{22}k_2 + \alpha_{23}k_3) \tag{14}$$

and

$$16D_3(\tilde{C}_{32} - \tilde{C}_{34}) = k_3(\alpha_{32}k_2 + \alpha_{33}k_3) \tag{15}$$

We then obtain the equation

$$\Theta k_2^4 + (A\alpha_{23}\alpha_{32} - 2A\alpha_{22}\alpha_{33} - B\alpha_{23}^2)k_2^2 + A^2\alpha_{33} = 0 \tag{16}$$

where $\Theta = \alpha_{33}\alpha_{22}^2 - \alpha_{22}\alpha_{23}\alpha_{32}$, $A = 16D_2(\tilde{C}_{21} - \tilde{C}_{23})$ and $B = 16D_3(\tilde{C}_{32} - \tilde{C}_{34})$.

We can obtain k_2 as the solution of Equation 16 because we know the values of $\tilde{C}_{21}$, $\tilde{C}_{23}$ and $\tilde{C}_{32}$ from the equilibrium diagram. We also obtain k_3 by substituting the value of k_2 into Equation 15.

The molar quantity of oxygen within the α-phase of Fig. 3b is given by

$$W_\alpha = \tfrac{1}{2}(\tilde{C}_{23} + \tilde{C}_{21})k_2 t^{1/2} f_c \tag{17}$$

and that of the β-phase is

$$W_\beta = \tfrac{1}{2}\tilde{C}_{32}k_3 t^{1/2} f_c \tag{18}$$

where f_c is the correction factor to put the normalized concentration into the actual content, i.e. $f_c = C_{ox} - C_o$. The molar quantity m of oxygen within the initial oxide film (per unit area) is given by Equation 6*. When the oxide film disappears ($t = t_s$), $m = W_\alpha + W_\beta$. The dissolution time for model 2 is therefore expressed by

$$t_s = \left(\frac{m}{\omega_\alpha + \omega_\beta}\right)^2 \tag{19}$$

where $\omega_\alpha = (f_c/2)(\tilde{C}_{23} + \tilde{C}_{21})k_2$ and $\omega_\beta = (f_c/2)\tilde{C}_{32}k_3$.

The time t_β required for the α-phase to vanish is given by model 1 (Equation 7), because oxygen dissolution in the β-phase is controlled by diffusion within the β-phase. Therefore

$$t_\beta = \frac{\pi}{D_3}\left(\frac{m}{2C_{\beta\alpha}}\right)^2 \tag{20}$$

where $C_{\beta\alpha}$ is the oxygen content of the β-phase adjacent to the α-phase as shown in Fig. 2.

$C_{\alpha 0}$, $C_{\alpha\beta}$ and $C_{\beta\alpha}$ in Fig. 2 were determined from the phase diagrams in Fig. 4, but C_{ox} was given by the stoichiometry. At that stage we obtained the molarity C as $C_w\rho_m/[M_o(100 - C_w)]$, where C_w is the weight percentile concentration, ρ_m the density of pure metal and M_o the atomic weight of oxygen. In converting the weight percentile to the molar concentration, we should take $(100 - C_w)$ in place of 100 because the solubility limit of oxygen for titanium is much greater than that of copper. Also, we take $C_o = 0$ mol m^{-3} for titanium. We ignored the δ-phase in Fig. 4b because it had no solubility for oxygen.

*Although titanium oxide has a solubility for oxygen, we assumed that ρ_{ox} is constant, regarding it as the stoichiometric compound (TiO).

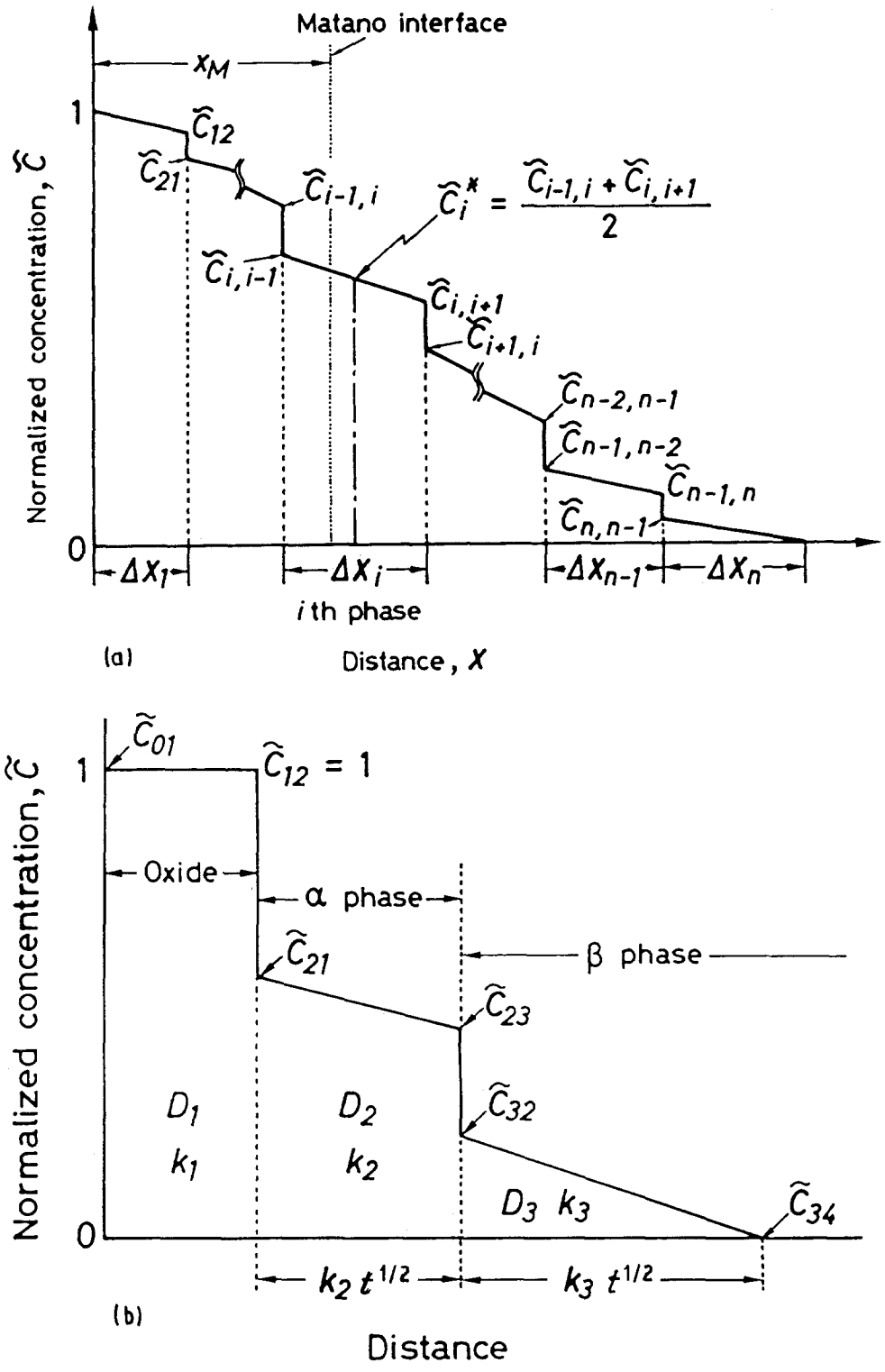

Figure 3 Concentration–distance curve in reaction diffusion: (a) formation of multiphase by mutual diffusion in binary system; (b) the case of $n = 3$, assuming that a diffused layer is not formed in the oxide film.

In Fig. 4, the solubility limit C_s of Cu was taken from published work [22, 23], as was the diagram of the Ti–O system [24]. The material constants used in the present study are listed in Table I [25–30].

Model 1 is applied to copper with a CuO film and α-titanium with a TiO film. On the other hand, model 2 is used in calculating t_s for β-titanium.

3. Calculated results

Fig. 5 shows the temperature dependence of the dissolution time t_s for CuO surface film during copper–copper diffusion bonding. Solid curves correspond to the case of $C_o = 0$ wt % and dotted curves are for $C_o = 1.0 \times 10^{-3}$ wt % (= 10.0 p.p.m.).

As shown in Fig. 4a, the solubility limit of copper for oxygen is relatively small. Also, industrially pure copper usually contains a little oxygen as a solute atom, even if it is called oxygen-free copper. Thus, the influence of the initial oxygen content C_o on the dissolution time is of great importance. As stated later, we used oxygen-free copper with $C_o = 10$ p.p.m. in the experiments. The dotted curves in Fig. 5 are more important, although the solid curves give the lower

TABLE I Material constants used in calculation

Symbol	Name	Material	Value	Reference
ρ_{ox}	Density of oxide	CuO	6400 kg m^{-3}	[25]
		Cu_2O	6040 kg m^{-3}	[25]
		TiO	4930 kg m^{-3}	[26]
		TiO_2	4250 kg m^{-3}	[26]
ρ_m	Density of pure metal	Cu	8930 kg m^{-3}	[27]
		α-Ti	4500 kg m^{-3}	[27]
		β-Ti	4400 kg m^{-3}	[27]
D_o	Frequency factor for oxygen diffusion	in Cu	7.595 m^2 s^{-1}	[28]
		in α-Ti	0.940 m^2 s^{-1}	[29]
		in β-Ti	4.5×10^{-5} m^2 s^{-1}	[30]
Q	Activation energy for oxygen diffusion	in Cu	229 kJ mol^{-1}	[28]
		in α-Ti	287 kJ mol^{-1}	[29]
		in β-Ti	151 kJ mol^{-1}	[30]

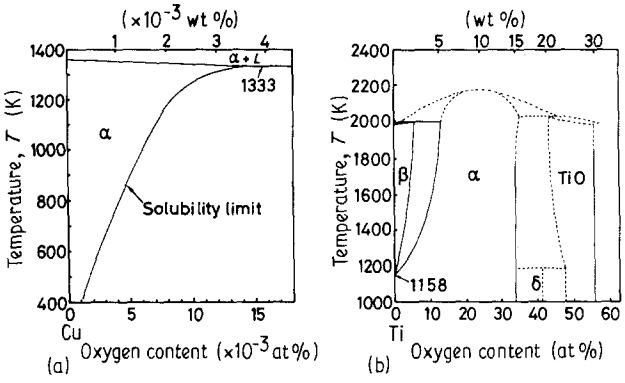

Figure 4 Phase diagrams: (a) Cu–O system. (b) Ti–O system.

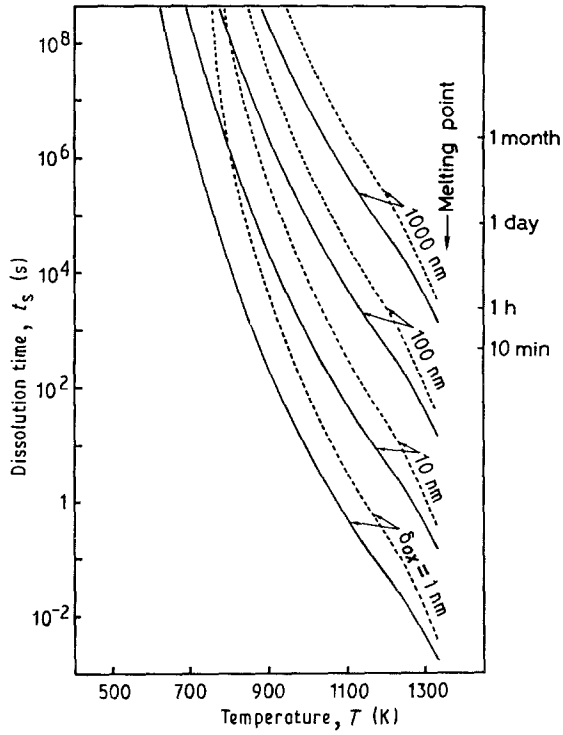

Figure 5 Temperature dependence of dissolution time of copper oxide film on copper (results calculated by model 1): (——) $C_o = 0$, (– – –) $C_o = 1.0 \times 10^{-3}$ wt %.

limit of t_s. The dissolution time is infinite at temperatures lower than T_s at which $C_o = C_s$. $T_s = 765$ K for $C_o = 10$ p.p.m. (cf. Fig. 4a). It follows that we get no metallic bonds when $T < T_s$ as long as we do nothing but keep the faying surfaces in soft contact with each other. In reality, copper–copper bonding cannot be achieved without large applied stress when $T < 750$ K [4, 5, 31]. This suggests that we need to break up the surface oxide film to attain the bonding process below T_s [11, 32]. (If the surface oxide film becomes spherical by itself to disperse on the bond-interface, the metallic bond can be achieved without pressure even if the temperature is lower than T_s.)

Even if we polish the specimen chemically in advance, we have an oxide film with a thickness of a few nanometres on the faying surface in air [33], so we need to examine the calculated results for $\delta_{ox} = 1$ to 10 nm in Fig. 5. In the temperature range higher than 1100 K, the dissolution time for $\delta_{ox} = 1$–10 nm is less than a few hundred seconds (for the specimen with $C_o \leqslant 10$ p.p.m.). This suggests that the bonding process above 1100 K instantly begins to progress as far as a polished surface is concerned. However, the dissolution time rapidly increases as the temperature decreases from 1100 K. For example, the dissolution time for $\delta_{ox} = 10$ nm and $T = 900$ K becomes several hours. In the temperature range lower than 900 K, it is rather hard to complete the bonding process under a low pressure which cannot break up the oxide film [11]. This is a reason why the temperature conditions for conventional copper–copper bonding are generally in the range of 1000 to 1273 K [4, 5, 31, 34].

Fig. 6 shows the temperature dependence of the dissolution time for titanium with TiO film. Solid lines in the temperature range lower than 1158 K are given by model 1 and correspond to the dissolution of the oxide film in α-titanium. On the other hand, those in the temperature range higher than 1158 K are given by model 2 for β-titanium and denoted by α + β, which means that the α-phase remains at the joint interface when the oxide film disappears. Dotted lines in Fig. 6 are obtained from Equation 20 and express the time taken for the oxygen to dissolve completely in β-titanium. We can thus know the period for the coexistence of α and β phases by the region lying between solid and dotted lines for the same δ_{ox}. As can

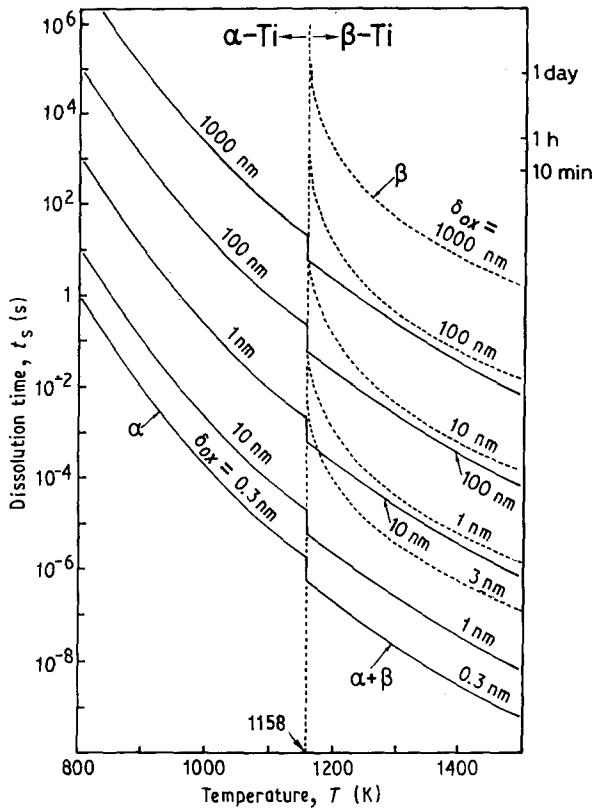

Figure 6 Temperature dependence of dissolution time of titanium oxide film on titanium ($C_o=0$). The solid curves for $T<1158$ K were calculated by model 1 and those for $T>1158$ K by model 2. The dotted curve for $T>1158$ K denotes the time when α-phase disappears.

be seen in Fig. 6, the dissolution time for $\delta_{ox} \leqslant 10$ nm is less than 1 s in the temperature range higher than 1000 K. This suggests that retardation of the bonding process is hardly observed in this temperature region [9]. In the β-phase region ($T > 1158$ K) we scarcely observe an incubation period due to the oxide film. However, in the α-phase region the dissolution time rapidly increases with decreasing temperature. When $T < 850$ K, t_s for $\delta_{ox} > 10$ nm is greater than 100 s. It is suggested that the oxide film has an influence on the commencement of the bonding process in the lower temperature region of the α-phase.

Several reports [4, 35] have indicated that it is rather difficult to achieve α-titanium bonding in the temperature range of $T < 950$ K. We can understand it if the specimens have a thick oxide film such as $\delta_{ox} > 100$ nm, but we know that the faying surface in diffusion bonding usually has only a thin oxide film. From Fig. 6, we find that it does not take a long time for a thin oxide film ($\delta_{ox} < 10$ nm) to dissolve completely (10 min is enough, even when the temperature is 800 K). The reports [4, 35] contradicts the results of Fig. 6 in the temperature range lower than 950 K. We need, therefore, to investigate the retardation of the bonding process in this temperature region.

4. Experimental procedure

4.1. Specimens

Copper and titanium specimens were prepared from oxygen-free copper and industrially pure titanium rods, respectively. The diameter of the specimens was 10 mm. The oxygen content of the copper specimens was 10 p.p.m. The purity of the titanium was 99.5 wt %. The faying surfaces were turned by lathe and polished by No. 1500 emery paper (or wet buff) before chemical polishing. One of a pair of specimens was fringed a little along the edge of the faying surface on the lathe.

The chemical polishing was performed as simply as possible according to Petzow [36]. The polishing time was up to 100 s. We took care that we did not make the surface curved by the chemical polishing. The maximum surface roughness R_{max} was less than 0.8 μm for all specimens. The specimens were finished so that the length was 13 mm. After the chemical polishing, some of the specimens were oxidized by dry air for 10 min at 673 K (or 473 K) for copper and 773 K for titanium in order to obtain a thick oxide film. The specimens without oxidizing treatment were exposed to dry air of 300 K for 1 h before the bonding tests.

4.2. Oxide films

The thickness of the surface oxide film was estimated by two methods. One was surface analysis by IMA and Auger electron spectroscopy (AES) [33]. The other was measurement of the change in weight with oxidation and was applied to the thick oxide film, because it was difficult to estimate the thickness of the thick oxide film of copper by IMA and AES. Foil which was polished under the same conditions was used for the latter method. The thickness of the polished foil was about 0.1 mm. We assumed that the change in weight of the foil was due to oxygen which made chemical bonds with the metal. At this stage we also assumed that the oxide film was uniform and consisted of the simple stoichiometric compound (CuO and TiO). The change in weight of the foil was measured to an accuracy of 1 μg.

X-ray analysis was carried out for the oxidized specimen. A thick oxide film was produced as for the oxidized copper specimens but no oxide films were observed on titanium as far as the X-ray analysis was concerned. A certain amount of oxide film appeared to occur on the titanium surface from IMA observation, but oxygen atoms dissolved in the α-phase more easily than they formed an oxide film. For titanium, we could not make a suitably thick oxide film by the oxidizing treatment [14].

For the thin oxide film, we estimated the thickness from the depth profile of the oxygen intensity, assuming that the sputtering rate was the same as that of the base metal. We could not exactly estimate the thickness of the oxide film because of broadening of the ion (electron) beam and selective sputtering. In measuring the depth profile, the intensity of oxygen decreased a little at first because of the broadening but increased immediately and decreased again. We assumed that the position where the intensity decreased to one-third of the maximum value was the interface between the oxide film and metal. Unfortunately, we could not identify the composition of the thin film by IMA and

AES. We thus regarded the thin films as CuO and TiO, although the oxide film of titanium might be TiO_2 according to Wanatabe and Horikoshi [9]. As a result, we got a thickness of 0.3 to 3 nm (about 1 nm) for thin copper oxide films and 20 ± 5 nm for TiO thin films.

From the X-ray analysis it was found that thick copper oxide film consisted of CuO and $6CuO \cdot Cu_2O$. However, we determined the thickness by regarding it as CuO (the amount of oxygen is the same even if we regard it as CuO). We obtained a thickness of 100 to 300 nm for the thick copper oxide films. We gave a certain latitude to the thickness of the oxide film because we could not estimate it exactly.

4.3. Bonding tests

We first applied pressure to specimens set in the holder up to 50 MPa for copper and 100 MPa for titanium by uniaxial stress. After that, the applied pressure was again reduced to 2 MPa after evacuating the air within the vacuum chamber. This first applied pressure was to ensure full contact over the faying surface.

According to Kragelsky and Demkin [37], the first pressure was not enough to attain full contact, i.e. there remained voids on the interface, but we could get full contact at the fringe of the faying surface. We could prevent the oxide film from escaping to the outside through the fringe.

We performed the bonding tests under a vacuum of 10^{-4} Pa. We heated the specimens by a molybdenum heater. The molybdenum heater was able to go up and down along the bonding jig [38]. We first applied it to the lower side. After that, we heated the specimens up to the bonding temperature by raising it to the upper side. We required about 60 s to attain the bonding temperature. We took the commencement of the bonding tests ($t = 0$) from heating the specimen up to the appointed temperature. At the same time, we gave a pressure of 5 MPa to the specimens. The temperature T was measured by a thermocouple in contact with the test piece and kept within ± 1 K during testing. The specimen was cooled under load quickly by lowering the molybdenum heater after turning it off [20, 38]. The cooling time to 200 K below the test temperature was about 40 s. The specimens joined by the bonding tests were bent to fracture and observed by SEM and electron probe microanalysis (EPMA) to examine the behaviour of the oxide film during bonding.

We could not perform the bonding tests for $t < 100$ s. When describing $t = 0$ in the following section, we mean that we cooled the specimen immediately after attaining the bonding temperature.

5. Experimental results

5.1. Copper

Fig. 7 shows the experimental results for copper–copper bonding compared with the calculated results. Fig. 7a is for a thin oxide film of $\delta_{ox} = 0.3$–3 nm and Fig. 7b for a thick oxide film of $\delta_{ox} = 100$–300 nm. The oxidizing treatment was given to both surfaces of the specimens. It is considered that the oxide film has not dissolved in the bulk in the region below the solid curves. It follows that a metallic bond must not occur in this region denoted by "unbonded". On the other hand, in the regions above the curves of $\delta_{ox} = 3$ nm for Fig. 7a and $\delta_{ox} = 300$ nm for Fig. 7b which are denoted by "no oxide", it is considered that the oxide film has completely dissolved in the bulk and a metallic bond can be formed. This consideration is supported by the experimental results indicated by the

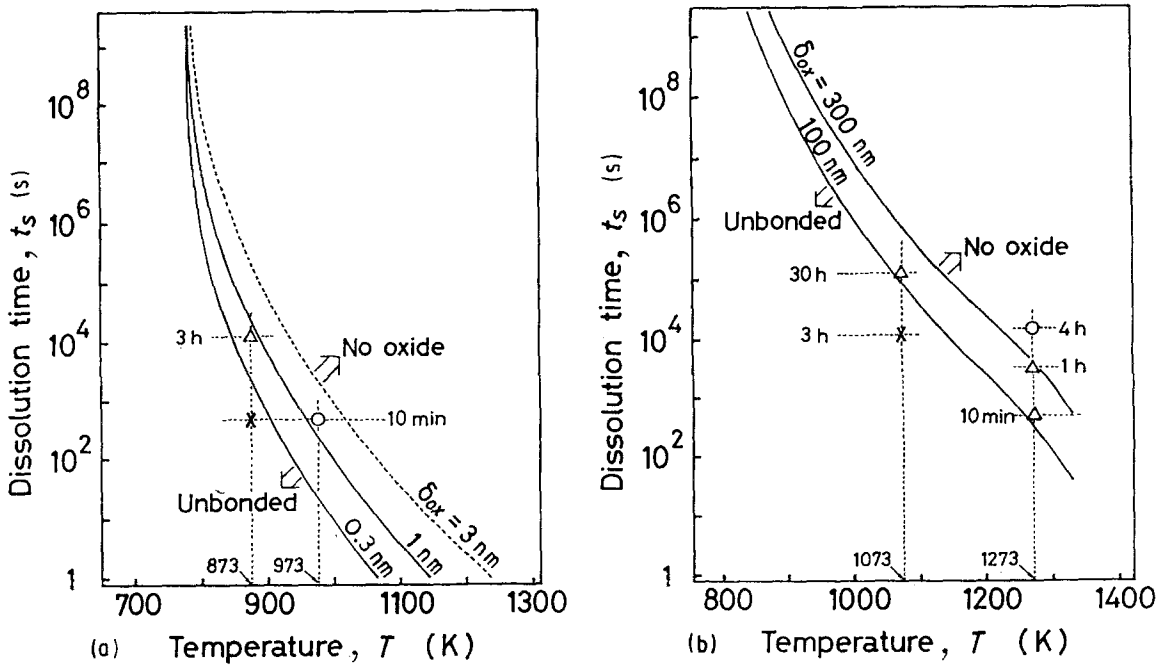

Figure 7 Verification of the dissolution process of copper oxide by experiments. (a) Thin oxide film with thickness $\delta_{ox} = 0.3$–3.0 nm. No. 1500 emery paper and chemical polish; (○) bonded, (△) poor bond, (×) unbonded. (b) Thick oxide film with $\delta_{ox} = 100$–300 nm; No. 1500 emery paper and heating in dry air at 673 K for 600 s; (○) bonded, (△) bonded with oxides, (×) unbonded.

three kinds of symbol. It was rather difficult to determine the dissolution time of the oxide film exactly by the analyses of AES, IMA and EPMA. We therefore used three kinds of symbol. When the fractured surface was dimpled (ductile fracture), we marked it with circles. We denoted no bonds by crosses, and used triangles when we got a poor bond (brittle fracture in Fig. 7a) or we observed oxide inclusions on the fractured surface (in Fig. 7b). In fact, the intensity (concentration) of oxygen at the bonded interface decreased considerably when it exhibited ductile fracture. When we had no bonds at all, we had a high intensity of oxygen adjacent to the faying surfaces in IMA (EPMA for the thick oxide film). However, a metallic bond tends to occur before the oxide film completely dissolves. That is, ductile fracture was exhibited very often in the region above the curve of $\delta_{ox} = 1$ nm in Fig. 7a. Ductile fracture was also observed in the region of $\delta_{ox} = 100$–300 nm in Fig. 7b, although the fractured surfaces had small oxide inclusions. The fracture mode appears to depend on the behaviour of the oxide film during bonding. Although we need to examine the behaviour of the oxide film in detail (cf. Fig. 8 below), we can say that the experimental results are in agreement with the calculated results of Fig. 7.

For a thin oxide film, the broadening and selective sputtering in the surface analyses did not permit us to get very positive evidence. The extent of the thickness from $\delta_{ox} = 0.3$–3 nm might be due to the broadening. We considered that, in fact, the thickness was less than 3 nm (so we denoted the calculated results for $\delta_{ox} = 3$ nm by a dotted line in Fig. 7). The experimental result denoted by a triangle in Fig. 7a exhibited a brittle fracture mode very similar to Fig. 10 in

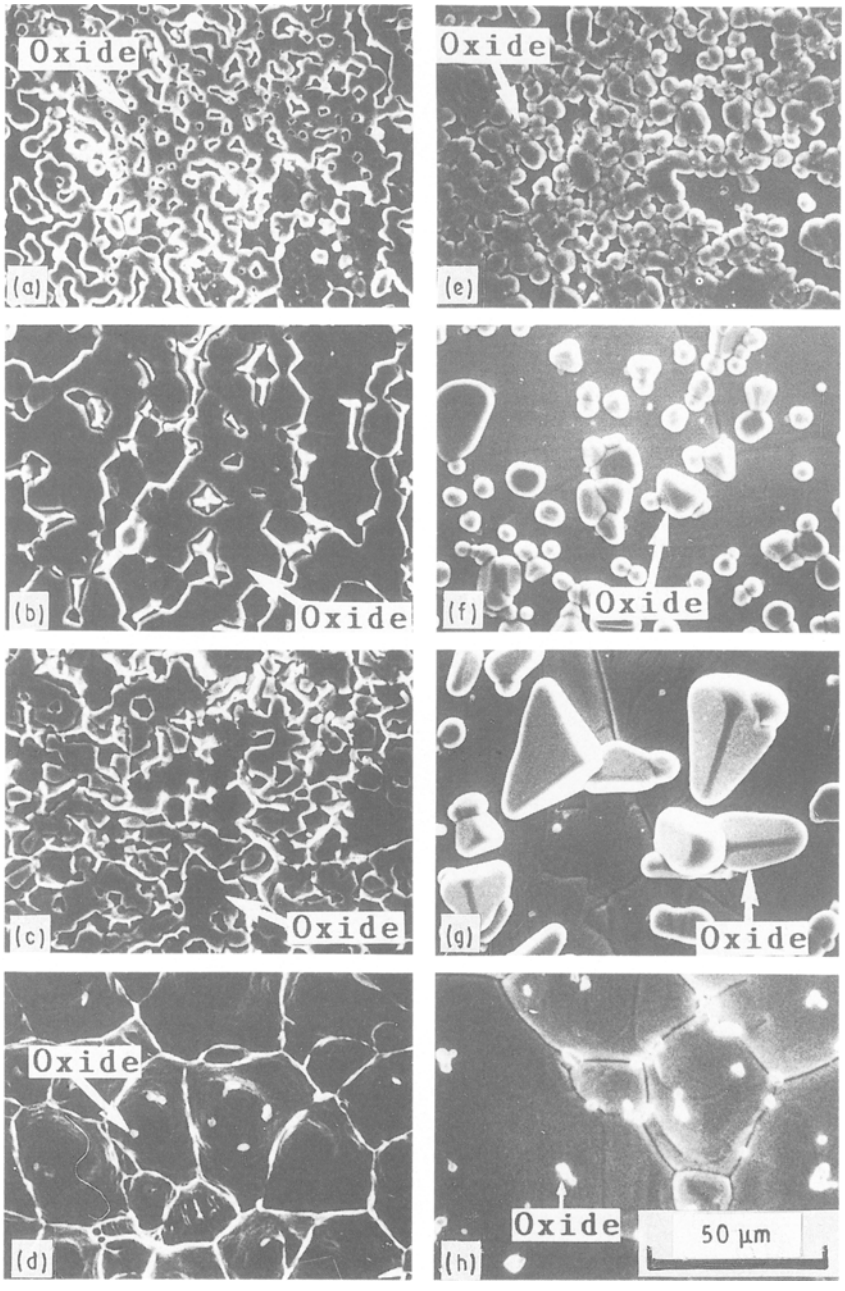

Figure 8 SEM observation of the behaviour of copper oxide film on contact area (fractured surface) and hole surface after diffusion bonding; $T = 1073$ K, $P = 5$ MPa, preheating in dry air at 673 K for 600 s (cf. Fig. 10a). Contact area: (a) 0.5 h, (b) 5 h, (c) 10 h, (d) 30 h. Hole surface: (e) 0.5 h, (f) 5 h, (g) 10 h, (h) 30 h.

Higgins and Munir [10]. This gives evidence of adhering through an oxide layer. This adhesion was poor, compared with the bond exhibiting the ductile fracture mode denoted by a circle.

Fig. 8 shows the results of SEM observation as to the behaviour of the thick oxide film during bonding. For this experiment, we made a hemispherical hole at the centre of the faying surface (cf. Fig. 10 below) before the oxidizing treatment. As seen in Fig. 8, the oxide layer does not dissolve uniformly. The behaviour of the oxide layer in the hole surface is quite different from that in the contacted area. The oxide film changes to many oxide particles (see Fig. 9) and then the oxide particles become once again large before vanishing. It was found from X-ray analysis that these particles consisted of CuO and Cu_2O (mainly $6CuO \cdot Cu_2O$). We supposed that the particles were due to the vapourization of the oxide layer. We then performed the annealing test described in Fig. 10a ($P = 5$ MPa). After testing, the oxide particles were observed on the chemically polished surface A as shown in Fig. 10b. A part of the oxide film obviously vapourizes during bonding. This is the reason why a local metallic bond is produced before the oxide film completely dissolves in the bulk. It is also considered that the vapourization makes it easy for the oxide film to dissociate. It follows that oxygen diffusion in the bulk controls the dissolution process of the oxide film. Grain boundary diffusion is negligible compared with lattice diffusion because the grain size was 10–20 nm. Oxide vapourization allows the oxygen concentration at the bond-interface to be uniform. It is concluded that model 1 (one-dimensional diffusion model) is valid for a copper oxide film.

5.2. Titanium

As stated above, Fig. 6 suggests that the oxide film easily dissolves in the region of $T > 1158$ K (β-titanium). This has also been suggested by Watanabe and Horikoshi [9]. In fact, bond formation easily began to occur in the bonding tests for $t = 0$, regardless of the oxidizing treatment. Oxide inclusions were not observed on either the hole surface or the contacted area in the temperature region higher than 1158 K. This was similar to the results reported by Ohashi and coworkers [11, 14]. Similar results were also obtained at $T = 1143$ K in the α-phase. These are shown in Fig. 11. The fracture mode is, however, different between the emery and buff polish. The surface asperity

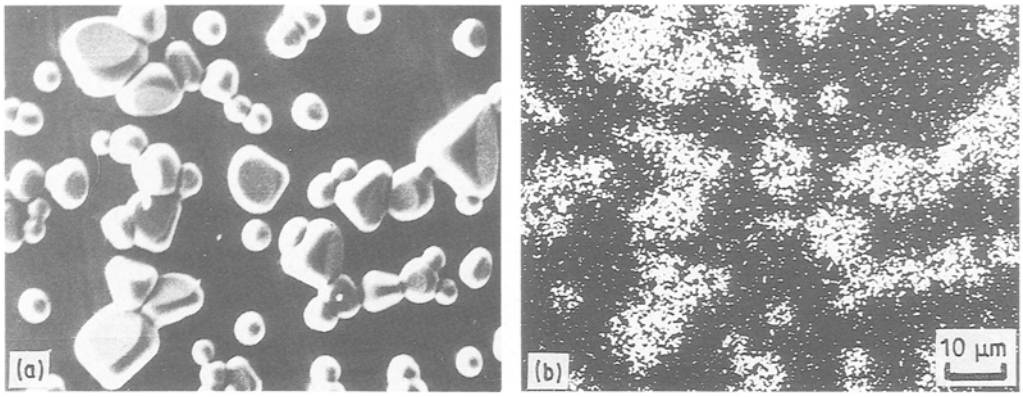

Figure 9 EPMA analysis of copper oxide particle on hole surface: (a) secondary electron image, (b) characteristic X-ray image of oxygen ($T = 1073$ K, $t = 5$ h).

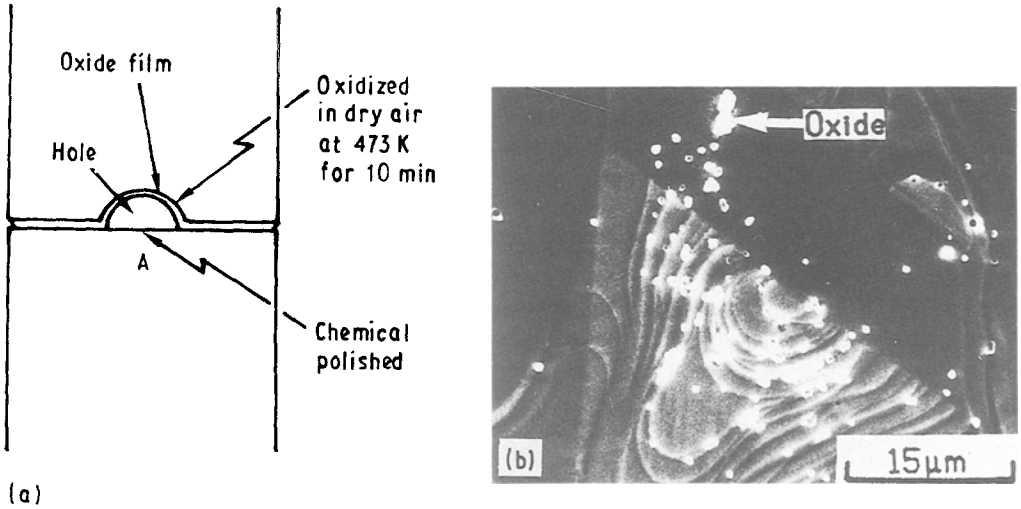

Figure 10 Experiments to verify the vaporization of copper oxide film during bonding: (a) schematic illustration of the test piece, (b) SEM photograph ($T = 1173$ K, $t = 1$ h).

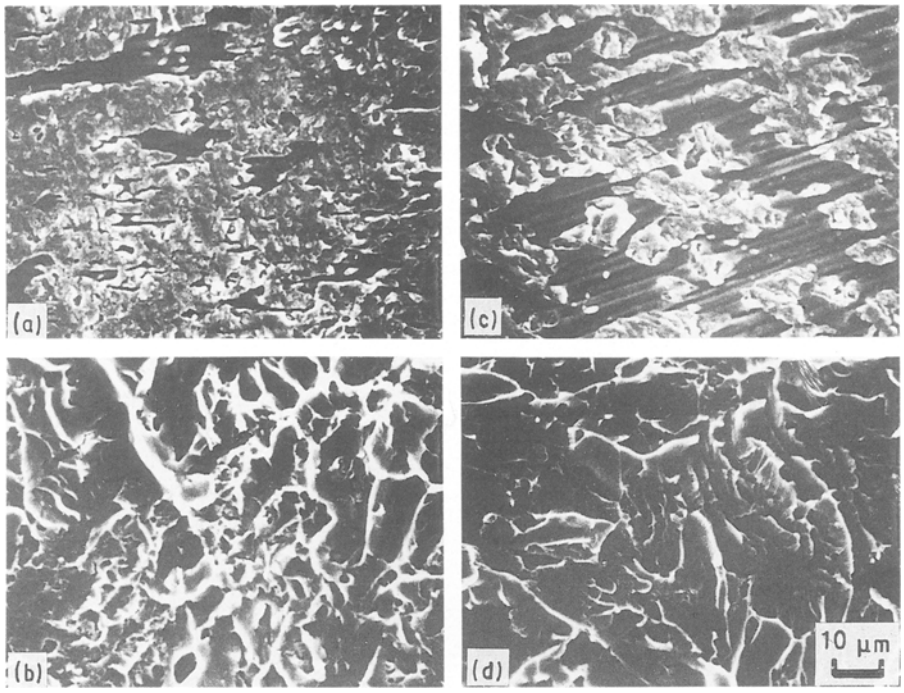

Figure 11 SEM observation of fractured surface after diffusion bonding of titanium: $T = 1143$ K, $P = 5$ MPa, $t = 0$. No oxidation: (a) emery polish (No. 1500), (b) buff polish. Oxidation in dry air at 773 K for 10 min: (c) emery polish, (d) buff polish.

appears to have an influence on the fracture mode. The influence is greater in the α-phase than in the β-phase. The thickness of the oxide layer was constant between the emery and buff polish within a factor of two*. Moreover, the real bonded area of no oxidation is larger than that of the oxidizing treatment. This is considered to be due to surface hardening by oxygen in solution.

Bonding tests in the temperature range lower than 1000 K exhibited more interesting results. The results are shown in Fig. 12, together with the calculated results of model 1. We used specimens with an oxide film of $\delta_{ox} = 20 \pm 5$ nm as stated in section 4. The results are arranged as Arrhenius plots. The time when the bond formation begins to occur is plotted. Circular symbols express the joint exhibiting a ductile fracture mode, triangles a joint with brittle fracture and crosses represent the unbounded state. The experimental points are on a straight line lying much above the calculated results.

It is obvious from Equation 7 of model 1 that t_s is proportional to $1/D$ if $(C_s - C_o)$ is constant against T. From Fig. 4b we know that the oxygen solubility of the α-phase is independent of temperature in the range $T < 1800$ K. We then find that t_s is proportional to $\exp(Q/RT)$, where Q is the activation energy of oxygen diffusion in α-titanium. We know that the slope of the calculated result corresponds to 287 kJ mol^{-1} (see Table I). In contrast, the apparent activation energy for the experimental results is 578 kJ mol^{-1}, much larger than that of model 1. This suggests that we need to consider another kinetic step as expressed by Equation 1 (dissociation process).

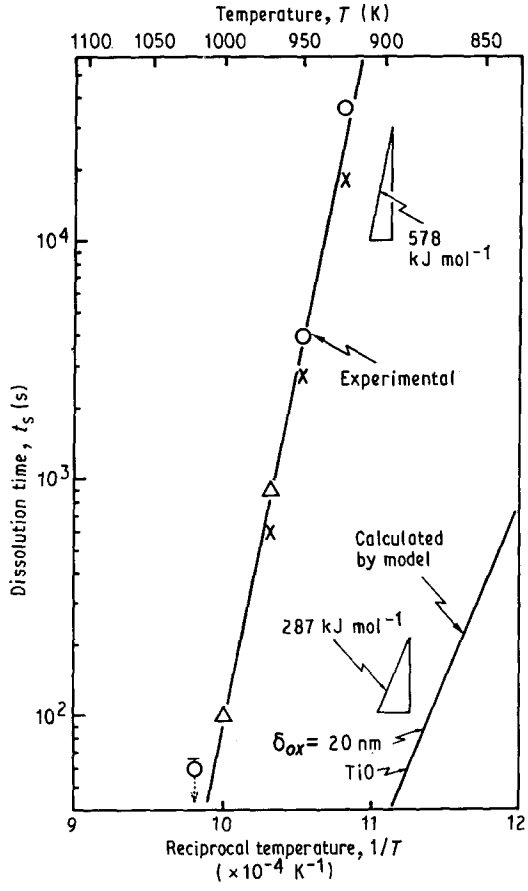

Figure 12 Experimental results to verify the temperature dependence of the dissolution time of titanium oxide film on titanium ($\delta_{ox} \simeq 20$ nm, $P = 5$ MPa): (○) bonded, (△) poorly bonded, (×) unbonded.

* We used only water in buff polishing. The intensity of oxygen in IMA and AES was broadened by the surface asperity. The oxide layer on the surface treated by No. 1500 emery seemed thicker than that of buff polishing. However, we could not exactly estimate the thickness (probably $\delta_{ox} = 20$–30 nm).

6. Discussion

We consider the kinetics of the dissociation of oxide film by analogy with solution reaction [18]. As described in Fig. 13, we assume that a region of activated state exists between the oxide film and the underlying metal. The thickness of the region δ^* is small enough to regard it as the interface between the oxide film and the metal. According to Moelwyn–Hughes [18], reactions for both dissociation and recombination are assumed to be proportional to the oxygen content within the reactive substance and to the surface area, S. We can therefore denote the dissociation and recombination rates by $\nu_s C_{ox}$ and $\nu_o C^*$, respectively, where C^* is the activated oxygen concentration at the interface between the oxide film and the metal, and ν_s and ν_o are constants (frequencies). The dissociation rate is expressed by

$$-\frac{dV^*}{dt}S = (\nu_s C_{ox} - \nu_o C^*)S\delta^* \quad (21)$$

where dV^*/dt is the molar quantity of oxygen having crossed unit area from the oxide film to the activated region in one second. When $C^* = C_s$, dC^*/dt is zero because the equilibrium state holds true [18], i.e.

$$\nu_s C_{ox} = \nu_o C_s \quad (22)$$

We also obtain the relationship $dV^*/dt = -(dC^*/dt)\delta^*$ by taking account of the dimensions and direction. Equations 21 and 22, therefore, lead to the rate equation expressed by

$$\frac{dC^*}{dt} = \kappa(C_s - C^*) \quad (23)$$

where κ is constant and equal to $\nu_s(C_{ox}/C_s)$. The solution of Equation 23 is represented by

$$C^* = C_s(1 - e^{-\kappa t}) \quad (24)$$

Equation 24 teaches us that C^* is nearly equal to C_s if κ is large enough, i.e. model 1 is valid in this case. On the other hand, if κ is small, C^* is approximately zero

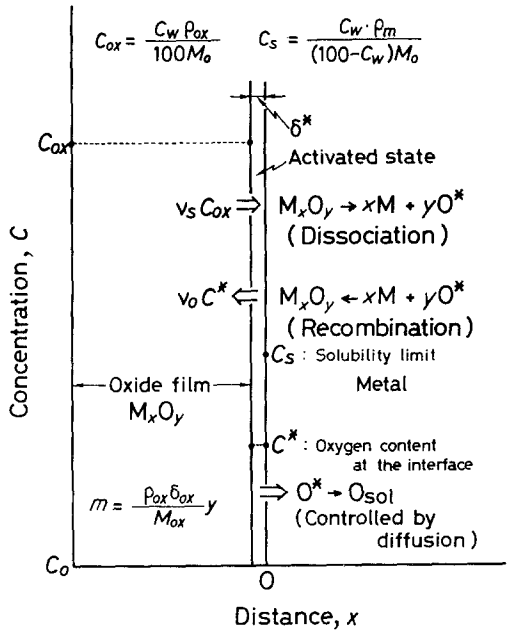

Figure 13 Schematic illustration of the series operation model.

before the oxide film has dissolved completely, i.e. Equation 23 is approximated by

$$\frac{dC^*}{dt} = \kappa C_s \quad (25)$$

where the thickness of the oxide film is assumed to be much less than the depth of the bulk. After integration of Equation 25 with respect to t, we obtain the total molar amount $C^*\delta^* (= \kappa\delta^* C_s t_s)$ of oxygen dissolving in the bulk. The dissolution time in this case is given by

$$t_s = \frac{m}{C_s \kappa \delta^*} \quad (26)$$

Now let us apply Equation 26 to the experimental results in Fig. 12. According to the theory of absolute reaction rate [39], κ is given by

$$\kappa = \kappa_o \exp\left(\frac{-\Delta H^*}{RT}\right) \quad (27)$$

where κ_o is the frequency factor and ΔH^* is the change in enthalpy for activation. From Fig. 12, $\Delta H^* = 578\ \mathrm{kJ\,mol^{-1}}$ and $\delta^*\kappa_o = 1.15 \times 10^{73}\ \mathrm{m\,s^{-1}}$ if we regard the oxide film as TiO; $\delta^*\kappa_o = 1.59 \times 10^{73}\ \mathrm{m\,s^{-1}}$ for TiO_2. Because we consider that δ^* is about 10^{-8} to 10^{-10} m, we notice that the values of κ_o are around $10^{82}\ \mathrm{s^{-1}}$. We know that the magnitude of 10^{82} is far too large, if we take account of the theory of the absolute reaction rate [39]. According to the theory, κ_o is given by

$$\kappa_o = \frac{kT}{h}\exp\left(\frac{\Delta S^*}{R}\right) \quad (28)$$

where k is the Boltzmann constant, h Planck's constant, and ΔS^* is the activation entropy [39]. The term kT/h is about 2×10^{13} when T is around 1000 K. If κ_o is of the order of $10^{82}\ \mathrm{s^{-1}}$, ΔS^* is nearly $1.3 \times 10^3\ \mathrm{J\,K^{-1}\,mol^{-1}}$. The true activation entropy must be one order of magnitude smaller than this value [39]. This contradiction must be due to neglecting the diffusion process to the bulk (Equation 2).

We need to consider the series operation of dissociation and diffusion. We assume that the number of the oxygens dissociated at the interface between the oxide film and the metal is equal to that of the oxygen dissolved in the bulk: $S\delta^*(dC^*/dt) = -S(dV^*/dt) = -SD(\partial C/\partial x)_{x=0}$, where $C_{x=0} = C^*$). This assumption leads to the equation

$$\frac{\partial C^*}{\partial x} = -h_r(C_s - C^*) \quad (29)$$

where $h_r = \delta^*\kappa/D$. Equation 29 is one of the boundary conditions for the one-dimensional diffusion equation $dC/dt = \partial^2 C/\partial x^2$.

We have $C = C_o$ at $x = \infty$ for $t > 0$ as another boundary condition and we also have $C = C_o$ at $x = 0 - \infty$ as the initial condition. The solution satisfying these conditions has been given by Crank [40], i.e.

$$\frac{C - C_o}{C_s - C_o} = \mathrm{erfc}(Z) - \exp(h_r x + z^2)\mathrm{erfc}(Z + z) \quad (30)$$

where $z = h_r(Dt)^{1/2}$, $Z = h_r x/2z$ and $\mathrm{erfc}(z) = 1 - \mathrm{erf}(z)$.

After integration of the flux $J(0, t) = -D(\partial C^*/\partial x)$ with respect to time t, we obtain the total amount M_t of diffusing oxygen having crossed unit area of the interface expressed by

$$M_t = \frac{C_s - C_o}{h_r}\left\{\exp(z^2)\mathrm{erfc}(z) - 1 + \frac{2}{\pi^{1/2}}z\right\} \quad (31)$$

Because $M_t = m$ when $t = t_s(C_o = 0)$, we obtain the equation

$$gz = f(z) - 1 \quad (32)$$

where $g = m/[C_s(Dt)^{1/2}] - 2/\pi^{1/2}$ and $f(z) = \exp(z^2)\mathrm{erfc}(z)$.

Now let us analyse the case where h_r is small enough so that z is much less than unity. In this case, we have $f(z)$ approximate to

$$f(z) = 1 - \frac{2}{\pi^{1/2}}z + z^2 - \frac{4}{3\pi^{1/2}}z^3 + \frac{1}{2}z^4 \quad (33)$$

by Taylor's theorem. If we take it down to the third term, we obtain $g = z - (2/\pi^{1/2})$ from Equation 32, i.e. $z = m/[C_s(Dt)^{1/2}]$. Since z has been defined as $(\delta^*\kappa/D)(Dt)^{1/2}$ we obtain the same solution as Equation 26 for $t = t_s$.

On the other hand, in the case where h_r is large enough so that z is much greater than unity, we have $f(z)$ approximate to

$$f(z) = \frac{1}{\pi^{1/2}}\left(\frac{1}{z} - \frac{1}{2z^3} + \frac{3}{2^2z^5}\right) \quad (34)$$

by using the asymptotic formula [40]. We know from Equation 34 that $f(z) \to 0$ when $z \to \infty$. We thus have $g = 0$ when $z \to \infty$, because $gz = -1$ in Equation 32. We then obtain the solution for model 1, i.e. Equation 7.

Now let us examine the experimental results in Fig. 12. We can estimate the values of t_s from Fig. 12, that is, $t_s = 3600$ s at $T = 950$ K and $t_s = 26\,000$ s at $T = 925$ K. Substituting these values into Equation 32 and assuming $\delta^* = 10^{-9}$ m, we can obtain the value of z for each t_s by the iteration method [41, 42]*. The solutions for z lead to the values of κ in Equation 27. We obtain ΔH^* and κ_o from two values of κ. We thus obtained $\Delta H^* = 581.54\ \mathrm{kJ\,mol^{-1}}$ and $\kappa_o = 8.547 \times 10^{29}\ \mathrm{s^{-1}}$ for TiO film and also $\Delta H^* = 583.02\ \mathrm{kJ\,mol^{-1}}$ and $\kappa_o = 1.439 \times 10^{30}\ \mathrm{s^{-1}}$ for TiO_2 film. (The value of m for TiO_2 is 1.379 times as large as that of TiO for the same value of δ_{ox}. This causes the difference in ΔH^* and κ_o.) Although the value of ΔH^* is nearly equal to the activation energy which is given by Equation 26, the values of κ_o from the model of series operation are far less than the frequency factors obtained from Equation 26. When κ_o is of the order of $10^{29}\ \mathrm{s^{-1}}$, we obtain the activation entropy of $\Delta S^* = 300\ \mathrm{J\,K^{-1}\,mol^{-1}}$ from Equation 28 in the temperature range around $T = 1000$ K. It is said that the activation entropy is less than $10\ \mathrm{J\,K^{-1}\,mol^{-1}}$ in common chemical reactions, but it often becomes pretty large for dissociation [39]. A ΔS^* of $300\ \mathrm{J\,K^{-1}\,mol^{-1}}$ is considered adequate.

The value of ΔH^* is much greater than that of oxygen diffusion. It is then necessary to consider the oxidizing reaction of titanium. The standard free energy change for $Ti + O_2 \to TiO_2$ is given by $\Delta G^0 = -910\,000 + 173T\ \mathrm{J\,mol^{-1}}$ and that of $Ti + (O_2/2) \to TiO$ is expressed by $-543\,000 - \Delta S^0 T\ \mathrm{J\,mol^{-1}}$, where ΔS^0 is the change in the entropy and its value is unknown (may be about -100 to $-200\ \mathrm{J\,K^{-1}\,mol^{-1}}$) [43, 44]. The standard enthalpy change ΔH^0 is -910 and $-543\ \mathrm{kJ\,mol^{-1}}$ for TiO_2 and TiO, respectively. When we discuss the value of ΔH^*, the absolute values of ΔH^0 become reference standards.

We need an activation energy greater than ΔH^0 to dissociate the titanium oxide independently. However, when dissociation is followed by dissolution in the titanium bulk, a value of $\Delta H^* = 910\ \mathrm{kJ\,mol^{-1}}$ may be enough to dissociate the oxide film. ΔH^* (about $580\ \mathrm{kJ\,mol^{-1}}$) is rather close to the absolute value of ΔH^0 for TiO ($= 543\ \mathrm{kJ\,mol^{-1}}$). If the oxide film consists of TiO, $\Delta H^* = 580\ \mathrm{kJ\,mol^{-1}}$ may be large enough with respect to dissociation from TiO to Ti + O*. This therefore suggests that the dissociation

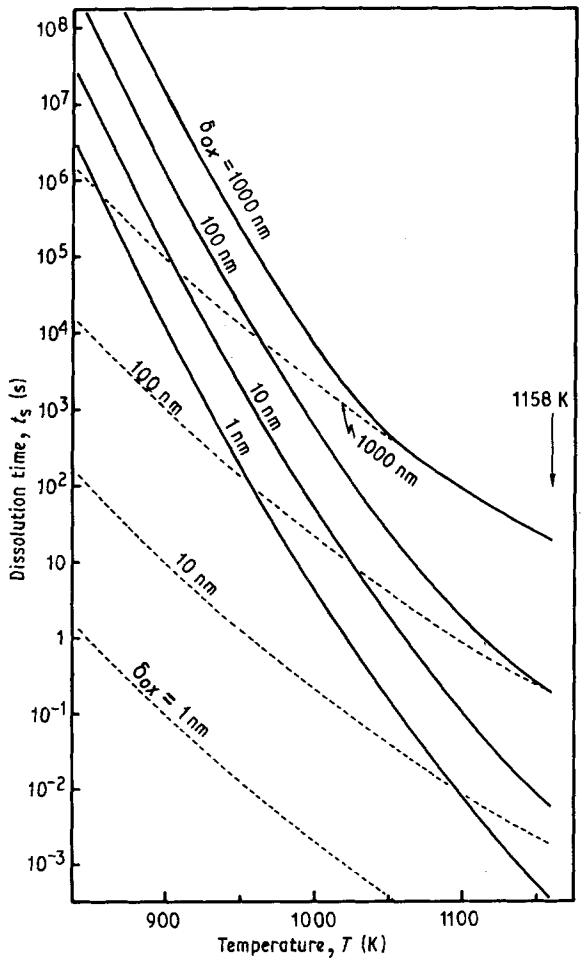

Figure 14 (——) Results calculated by the series operation model for α-Ti ($T < 1158$ K, oxide film TiO) to show the temperature dependence of dissolution time, compared with (---) results calculated by model 1.

* We consider that δ^* is less than δ_{ox} and greater than the magnitude of the lattice constant. In the iteration method, the initial value of z was obtained by using Equation 26, i.e. $z = (\kappa\delta^*/D)(Dt_s)^{1/2}$, where $\kappa\delta^* = t_s C_s/m$.

TABLE II Variation of κ and h_r with T (for TiO)

	T(K)				
	800	900	1000	1100	1150
κ (s^{-1})	9.1×10^{-18}	1.5×10^{-13}	3.5×10^{-10}	2.1×10^{-7}	3.3×10^{-6}
h_r (m^{-1})	5.3×10^{1}	7.3×10^{3}	3.7×10^{5}	9.4×10^{6}	3.8×10^{7}

process occurs after the oxide film changes to TiO, even if it has a composition such as TiO_2 [45].

We can solve for the dissolution time t_s by the series operation model because we have obtained the values of $\delta^*\kappa_0$ and ΔH^*. i.e. t_s is given by

$$t_s = \frac{\pi}{4Dh_r^2}\left[\frac{mh_r}{C_s} + 1 - f(z)\right]^2 \quad (35)$$

where $z = h_r(Dt_s)^{1/2}$. We inevitably need the iteration method to obtain the value of t_s.

Fig. 14 shows the temperature dependence of the dissolution time for titanium oxide (TiO) calculated by the series operation model (solid lines). The calculated results for model 1 are also shown as dotted lines. The solid lines approximate to the dotted lines with increasing temperature. The temperature where they are close to each other decreases with increasing δ_{ox}. For $\delta_{ox} \geqslant 20$ nm, the results calculated by the series operation model become nearly equal to those of model 1 before the temperature is greater than 1150 K. However, as far as we see from Fig. 14, model 1 is not valid at temperatures lower than 1100 K.

The calculated values of κ and h_r are shown in Table II. We find that model 1 is valid only when h_r is greater than 10^7. Also we see that h_r is greater than unity even at $T = 800$ K. We should not use Equation 26 until the temperature is somewhat lower than 800 K.

The series operation model explains why it is very difficult in the temperature range lower than 900 K to complete the diffusion bonding of titanium [4, 5] and the sintering of titanium powder [9] if the titanium has an oxide film on the faying surface.

7. Conclusions

The dissolution process of surface oxide film during the diffusion bonding of similar metals (Cu–Cu and Ti–Ti) has been examined numerically and experimentally, for the purpose of comprehending the role of the oxide film in the bonding process. With respect to a copper oxide film on copper, model 1 (the dissolution process controlled by oxygen diffusion) is valid because the oxide film is vapourized at the high temperature. On the other hand, model 1 is not always valid for a titanium oxide film on titanium. In the temperaure range lower than 1100 K, a new model involving series operation of dissociation and diffusion is necessary in order to comprehend the dissolution process of the surface oxide film during titanium bonding. However, the dissolution time for $T > 1100$ K can be estimated by model 1 because the titanium usually has a surface oxide film of a few tens of nanometres in air [9, 31, 33]. The dissociation process occurs more rapidly than the diffusion process in the temperature region $T > 1158$ K ($h_r = \kappa/D = 10^7$). Therefore, model 2 (dissolution process controlled by reaction diffusion) is considered to be valid for β-titanium although it was not verified exactly by the experiments.

It is widely known that the conventional diffusion bonding of metals becomes impossible when the bonding temperature is lower than the homologous temperature $T/T_m = 0.5$, where T_m is the melting point [4, 5] (for titanium, $T = 996$ K corresponds to $T/T_m = 0.5$). This is considered to be caused by deceleration of the dissociation rate of the oxide film with decreasing temperature. This can be quantitatively indicated by the series operation model proposed in the present study. We can at least say that the series operation model is able to estimate the impossible region for conventional diffusion bonding of titanium. Finally, for metals and alloys with a stable surface oxide film such as aluminium, zirconium and hafnium, we consider that the series operation model is necessary to estimate the dissolution time.

References

1. K. NISHIGUCHI and Y. TAKAHASHI, *Q. J. Jpn. Welding Soc.* **3** (2) (1985) 303.
2. B. DERBY and E. R. WALLACH, *Met. Sci. J.* **16** (1982) 49.
3. F. B. SWINKELS and M. F. ASHBY, *Acta Metall.* **29** (1981) 259.
4. K. MASUMOTO, K. TAMAKI, K. TERAI and Y. NAGAI, *Bull. Jpn. Inst. Met.* **9** (1970) 653.
5. T. ENJO and K. IKEUCHI, *ibid.* **21** (1982) 959.
6. Z. A. MUNIR, *Welding J.* **62** (12) (1983) 333s.
7. W. A. BRYANT, *ibid.* **54** (12) (1975) 433s.
8. P. J. HEATH and P. E. EVANS, *J. Mater. Sci.* **9** (1974) 1955.
9. T. WATANABE and Y. HORIKOSHI, *Int. J. Powder Metall. Tech.* **12** 3 (1976) 209.
10. P. K. HIGGINS and Z. A. MUNIR, *Powder Metall.* **21** (4) (1978) 188.
11. O. OHASHI, K. TANUMA and T. KIMURA, *Q. J. Jpn. Welding Soc.* **4** (1) (1986) 53.
12. T. ENJO, K. IKEUCHI and K. FURUKAWA, *Trans. JWRI* **14** (1) (1985) 115.
13. Z. A. MUNIR, *J. Mater. Sci.* **14** (1979) 2733.
14. O. OHASHI, K. TANUMA and K. YOSHIHARA, *Q. J. Jpn. Welding Soc.* **3** (3) (1985) 41.
15. J. R. MANNING, in "Diffusion Kinetics for Atoms in Crystals" 1st. Edn (Van Nostrand, London, 1968) p. 18.
16. K. P. GUROV, V. N. PIMENOV and Y. E. UGASTE, *Fiz. Metal. Metalloved.* **32** (1) (1971) 103.
17. Y. FUNAMIZU and K. WATANABE, *J. Jpn. Light Met. Soc.* **25** (5) (1975) 179.
18. E. A. MOELWYN-HUGHES, "The Kinetics of Reaction in Solution", 2nd Edn (Oxford University Press, London, 1947) p. 357.
19. P. G. SHEWMON, "Diffusion in Solids" (McGraw-Hill, New York, 1963) p. 12.
20. K. NISHIGUCHI, Y. TAKAHASHI and A. SEO, *Q. J. Jpn. Welding Soc.* **8** (3) (1990) 40.
21. G. B. GIBBS, *J. Nuclear Mater.* **20** (1966) 303.
22. F. N. RHINES and C. H. MATHEWSON, *Trans. Amer. Inst. Min. Met. Eng.* **111** (1934) 337.

23. "Metals Handbook", 3rd Edn, edited by Japan Metal Society (Maruzen, Tokyo, 1960) p. 1292.
24. "Metal Data Book", edited by Japan Metal Society (Maruzen, Tokyo, 1974) p. 479.
25. B. TAMAMUSHI *et al.*, in "Dictionary of Physics and Chemistry", 3rd Edn (Yuwanami-shoten, Tokyo, 1976) p. 515.
26. *Idem, ibid.* p. 514, or "Handbook of Physics and Chemistry", 67th Edn, edited by R. C. Weast *et al.* (CRC Press, USA, 1986–1987) p. B-140.
27. "Metal Data Book", edited by Japan Metal Society (Maruzen, Tokyo, 1974) p. 9.
28. F. BOUILLON and J. ORSZAGH, *Soc. Chim. Belg.* **78** (1969) 445, or in *Diffusion Data* **4** (2) (1970) 192.
29. V. I. TIKHOMIROV and V. I. DXACHOV, *Zh. Prikl. Khim.* **40** (1967) 2405, or *Diffusion Data* **2** (3/4) (1968) 308.
30. L. E. SOKIRIANSKI, D. V. IGNATOV and A. Y. SHINYAEV, *Fiz. Metal. Metalloved.* **28** (2) (1969) 287.
31. O. OHASHI and T. HASHIMOTO, *J. Jpn. Welding Soc.* **45** (1976) 295.
32. R. F. TYLECOTE, D. HOWD and J. E. FURMIDGE, *Br. Welding J.* (1958) 21.
33. O. OHASHI, K. TANUMA, and K. YOSHIHARA, *Q. J. Jpn. Welding Soc.* **3** (1) (1985) 153.
34. B. DERBY and E. R. WALLACH, *J. Mater. Sci.* **19** (1984) 3140.
35. W. H. KING and W. A. OWCZARSKI, *Welding J.* **46** (1967) 289s.
36. G. PETZOW, in "Metallographisches Atzen" (Gebruder Borntraeger, Berlin, Japanese edition published by AGNE, Tokyo, 1976) p. 63 for Cu, p. 95 for Ti.
37. I. V. KRAGELSKY and N. B. DEMKIN, *Wear* **3** (1960) 170.
38. K. NISHIGUCHI and Y. TAKAHASHI, *Q. J. Jpn. Welding Soc.* **3** (2) (1985) 309.
39. S. GLASSTONE, K. J. LAIDLER and H. EYRING, in "The Theory of Rate Processes" (McGraw-Hill, New York, 1964) pp. 1 and 21.
40. J. CRANK, "The Mathematics of Diffusion", 2nd Edn (Clarendon Press, Oxford, 1975) p. 36.
41. G. D. SMITH, in "Numerical Solution of Partial Differential Equations" (Oxford University Press, Oxford, 1965) p. 29.
42. H. TOKAWA, in "Numerical Analysis and Simulation" (Kyouritsu, Tokyo, 1976) p. 65.
43. D. R. GASKELL, "Introduction to Metallurgical Thermodynamics", 2nd Edn (McGraw-Hill, New York, 1981) p. 586.
44. O. KUBASCHEWSKI and C. B. ALCOCK, "Metallurgical Thermochemistry", 5th Edn (Pergamon, Oxford, 1979) p. 316.
45. P. STROBEL and Y. L. PAGE, *J. Mater. Sci.* **17** (1982) 2424.

Received 20 September 1990
and accepted 7 March 1991